Supporting Information

Chen et al. 10.1073/pnas.1311772110

SI Results

Repetitive Transcranial Magnetic Stimulation Results—Reliability-Related Analyses. We examined the influence of two potential confounding factors with regard to the effects of repetitive transcranial magnetic stimulation (rTMS). When we included a between-subject experiment "sequence" factor [i.e., posterior middle frontal gyrus (pMFG) rTMS first vs. anterior MFG (aMFG) rTMS first] in the ANOVAs above, there was no significant session × sequence interaction for either of our key signal amplitude measures [low-frequency (LF) signal amplitude: $F_{2,19} = 1.56$, $P > 0.24$; high-frequency (HF) signal amplitude: $F_{2,19} = 0.64$, $P > 0.54$], whereas the main effect of session persisted (LF signal amplitude: $F_{2,19} = 7.3$, $P = 0.004$; HF signal amplitude: $F_{2,19} = 5.59$, $P > 0.012$). Thus, our counterbalancing procedure worked as intended. Next, we examined whether the observed LF and HF signal amplitude alterations with pMFG rTMS reflects a change greater than variation between repeated resting-state scans. Consistent with prior findings on the reliability of default mode network (DMN) resting signal (1), if we used the "session 1" resting scan in place of the pre-rTMS baseline resting scan, we found similarly significant effects of session for LF ($F_{2,20} = 17.73$, $P < 0.001$) and HF ($F_{2,20} = 4.8$, $P = 0.02$) signal amplitudes as reported above.

SI Methods

Structural MRI. A high-resolution T1-weighted spoiled grass gradient recalled inversion recovery 3D MRI sequence was used: inversion time (TI) = 400 ms, repetition time (TR) = 6.2 ms; echo time (TE) = 2 ms; flip angle = 15°; 25.6-cm field of view; 146 coronal slices (1.2-mm slice thickness); 256 × 256 matrix.

General Scan Parameters. We used a 1.5T GE Signa Excite scanner at Stanford University. Twenty-nine axial slices (4 mm thick) covered the whole brain, using a T2-weighted gradient-echo spiral-in/out pulse sequence (TE = 40 ms; flip angle = 85°; 22-cm field of view; 64 × 64 matrix, and one interleave; TR = 2,000 ms) (2). Resting-state scans were acquired with no pause between volumes, whereas concurrent TMS/fMRI scans were acquired with a 400-ms pause between volumes to allow interleaving of single TMS pulses (3). An automated high-order shimming method based on spiral acquisitions was used before acquiring fMRI scans (4).

fMRI Data Preprocessing. A linear shim correction was applied separately for each slice during reconstruction using a magnetic field map acquired automatically by the pulse sequence at the beginning of the scan (5). Preprocessing using FSL (http://www.fmrib.ox.ac.uk/fsl/) (6) included realignment, 6-mm FWHM Gaussian kernel smoothing, removal of linear temporal trends, and correction for physiological noise using measures of heart rate and respiration (7, 8). For resting-state scans, motion parameters and white matter/cerebrospinal fluid time courses were also regressed out. High-resolution structural scans were normalized to standard MNI space using a nonlinear high-resolution warp normalization method (FNIRT) to the matching Montreal Neurological Institute (MNI) 152 brain template (6).

We followed standard preprocessing methods. No participants had movement greater than 3 mm of translation or 3° of rotation. We also ruled out that differences in head motion (9, 10) or physical sensation during TMS to different sites confounded our findings, by calculating the maximum peak-to-peak excursion and rms fluctuation for all six motion parameters during resting-state scans and quantifying self-reported discomfort, and found no differences between stimulation targets across scans (all $P > 0.23$).

1. Van Dijk KR, et al. (2010) Intrinsic functional connectivity as a tool for human connectomics: Theory, properties, and optimization. *J Neurophysiol* 103(1): 297–321.
2. Glover GH, Law CS (2001) Spiral-in/out BOLD fMRI for increased SNR and reduced susceptibility artifacts. *Magn Reson Med* 46(3):515–522.
3. Bohning DE, et al. (1998) Echoplanar BOLD fMRI of brain activation induced by concurrent transcranial magnetic stimulation. *Invest Radiol* 33(6):336–340.
4. Kim DH, Adalsteinsson E, Glover GH, Spielman DM (2002) Regularized higher-order in vivo shimming. *Magn Reson Med* 48(4):715–722.
5. Glover GH, Lai S (1998) Self-navigated spiral fMRI: Interleaved versus single-shot. *Magn Reson Med* 39(3):361–368.
6. Jenkinson M, Beckmann CF, Behrens TE, Woolrich MW, Smith SM (2012) Fsl. *Neuroimage* 62(2):782–790.
7. Glover GH, Li TQ, Ress D (2000) Image-based method for retrospective correction of physiological motion effects in fMRI: RETROICOR. *Magn Reson Med* 44(1):162–167.
8. Chang C, Glover GH (2009) Effects of model-based physiological noise correction on default mode network anti-correlations and correlations. *Neuroimage* 47(4):1448–1459.
9. Van Dijk KR, Sabuncu MR, Buckner RL (2012) The influence of head motion on intrinsic functional connectivity MRI. *Neuroimage* 59(1):431–438.
10. Power JD, Barnes KA, Snyder AZ, Schlaggar BL, Petersen SE (2012) Spurious but systematic correlations in functional connectivity MRI networks arise from subject motion. *Neuroimage* 59(3):2142–2154.

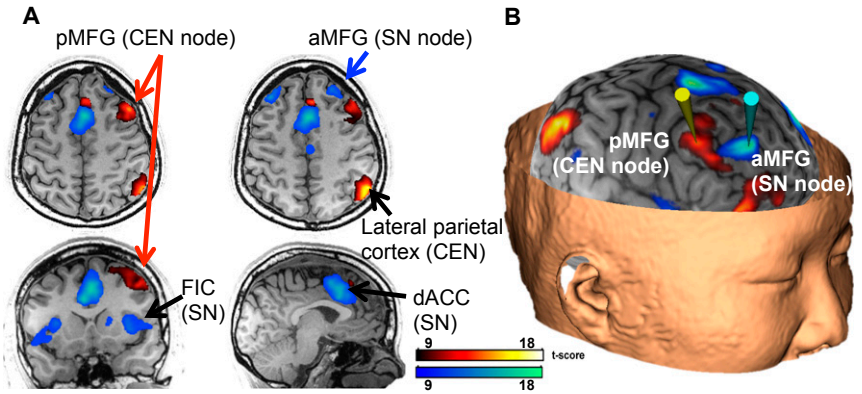

Fig. S1. Identification of stimulation sites for an individual subject. (*A*) Independent component analysis (ICA)-identified networks from a separate healthy subject cohort ($n = 38$) were used to map the fronto-parietal central executive network (CEN) (warm-color spectrum) and cingulo-opercular salience network (SN) (cool-color spectrum). Maps of these networks were reverse-normalized into each subject's native anatomical space and coregistered to their head using frameless stereotactic neuronavigation. The pMFG node of the CEN is indicated with red arrows, whereas the aMFG node of the SN is indicated with a blue arrow. Also shown are the parietal portion of the CEN and the dorsal anterior cingulate (dACC) and fronto-insular cortical (FIC) portions of the SN. (*B*) Example stimulation sites in native subject space, along with stimulation trajectories estimated to be perpendicular to the local orientation of the gyrus, were then selected according to the peak of ICA connectivity within the respective cluster: pMFG (yellow cone), aMFG (cyan cone).

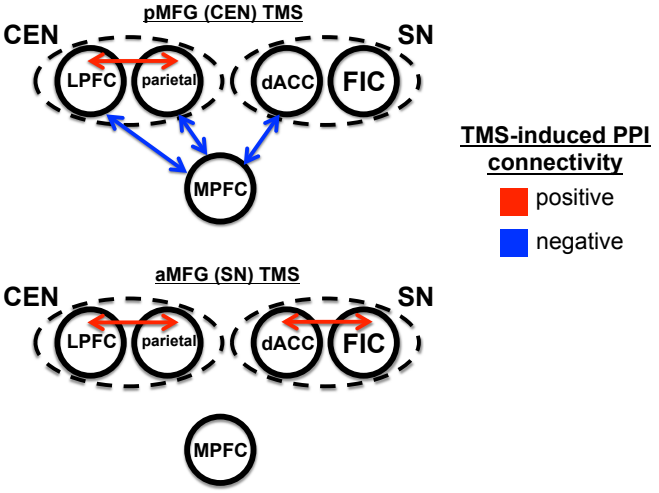

Fig. S2. Schematic diagram of the single-pulse TMS-induced psychophysiological interaction analysis (PPI) results observed in this study, between regions within the CEN [lateral prefrontal (LPFC), parietal], the SN (dACC, FIC), and the medial prefrontal cortex (MPFC) component of the DMN.

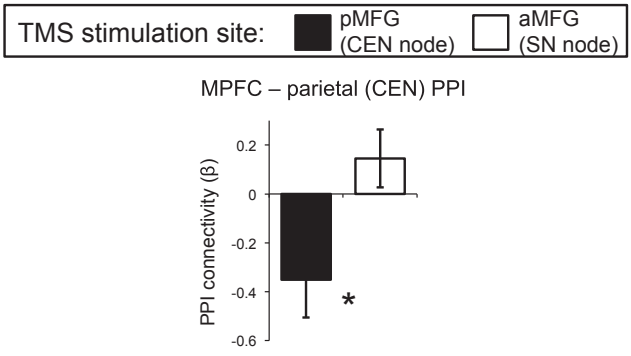

Fig. S3. Single-pulse excitatory TMS to the pMFG (CEN node), but not to the aMFG (SN node), resulted in negative PPI connectivity between the parietal node of the CEN and MPFC node of the DMN.

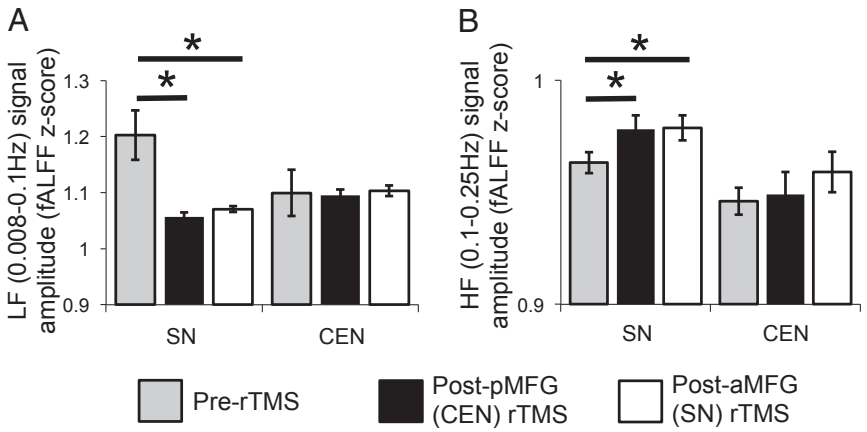

Fig. S4. No significant differences between effects of pMFG or aMFG rTMS were found for resting-state signal amplitude within the CEN or SN, although rTMS to either target led to decreased LF (*A*) and increased HF signal amplitude (*B*) in the SN.

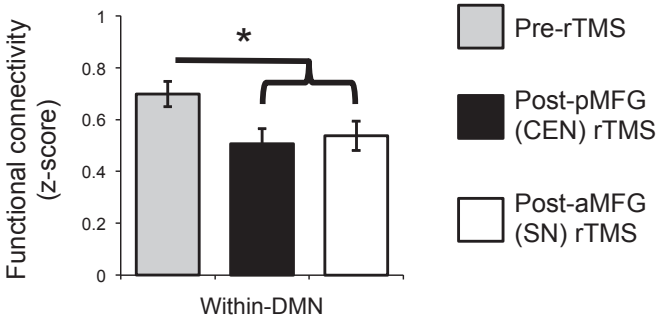

Fig. S5. No significant differences between effects of pMFG or aMFG rTMS were found for resting-state DMN functional connectivity, although rTMS to either target led to decreased connectivity in the DMN.

Table S1. Network a priori regions of interest

Region of interest	No. of voxels (mm^3)	Center-of-mass MNI coordinates (x, y, z)	Brodmann's area (BA)
MPFC	999 (7,992)	(−2, 53, 5)	9/10/11/32
Posterior cingulate cortex	1,006 (8,048)	(−1, −61, 16)	23/29/30/31
dACC	999 (7,992)	(1, 9, 52)	24/32/6
FIC	996 (7,968)	(49, 13, −6)	13/44/45/47
LPFC	994 (7,952)	(38, 16, 50)	6/8/9/46
Lateral parietal cortex	1,009 (8,072)	(45, −64, 40)	7/39/40